energies

MDPI

Article

The Synthesis and Electrochemical Performance of Si Composite with Hollow Carbon Microtubes by the Carbonization of Milkweed from Nature as Anode Template for Lithium Ion Batteries

Eun Hyuk Chung [1,*], Jong Pil Kim [2], Hyun Gyu Kim [2], Jae-Min Chung [3], Sei-Jin Lee [4], Jong-Seong Bae [2] and Euh Duck Jeong [2,*]

1 Department of Architectural Engineering, 37, Nakdong-daero 550beon-gil, Saha-gu, Busan 49315, Korea
2 Division of Analysis & Research, Korea Basic Science Institute, 1274-1, Jisa-dong, Gangseo-gu, Busan 46742, Korea; jpkim@kbsi.re.kr (J.P.K.); hhgkim@kbsi.re.kr (H.G.K.); jsbae@kbsi.re.kr (J.-S.B.)
3 Korea National Arboretum, 415 Gwangneungsumokwonro, Soeul-up, Pocheon-city 11186, Gyeonggi-do, Korea; rhuso@korea.kr
4 Jeonju Center, Korea Basic Science Institute, 634-18, Geumam-dong, Deokjin-gu, Jeonju-si 54907, Jeollabuk-do, Korea; lsj@kbsi.re.kr
* Correspondence: echung43@gmail.com (E.H.C.); edjeong@kbsi.re.kr (E.D.J.)

Received: 31 August 2020; Accepted: 24 September 2020; Published: 1 October 2020

Abstract: It has been reported that improving electrical conductivity and maintaining stable structure during discharge/charge process are challenge for Si to be used as an anode for lithium ion batteries (LIB). To address this problem, milkweed (MW) was carbonized to prepare hollow carbon microtubes (HCMT) derived from biomass as an anode template for LIB. In order to improve electrical conductivity, various materials such as chitosan (CTS), agarose, and polyvinylidene fluoride (PVDF) are used as carbon source (C1, C2, and C3) by carbonization. Carbon coated HCMT@Si composits, HCMT@Si@C1, HCMT@Si@C1@C2, and HCMT@Si@C1@C3, have been successfully synthesized. Changes in structure and crystallinity of HCMT@Si composites were characterized by using X-ray diffraction (XRD). Specific surface area for samples was calculated by using BET (Brunauer–Emmett–Teller). Also, pore size and particle size were obtained by particle and pore size analysis system. The surface morphology was evaluated using high resolution scanning electron microscopy (HR-SEM), Field Emission transmission electron microscopy (TEM). The thermal properties of HCMT@Si composites were analyzed by thermogravimetric analysis (TGA). Our research was performed to study the synthesis and electrochemical performance of Si composite with HCMT by the carbonization of natural micro hollow milkweed to form an inner space. After carbonization at 900 °C for 2 h in N_2 flow, inner diameter of HCMT obtained was about 10 μm. The electrochemical tests indicate that HCMT@Si@C1@C3 exhibits discharge capacity of 932.18 mAh/g at 0.5 A/g after 100 cycles.

Keywords: biomass; milkweed (MW); hollow carbon microtubes (HCMT); lithium-ion battery

1. Introduction

It has been known Silicon (Si) has many advantages such as high theoretical capacity (4200 mAh/g), non-toxic, low cost, and abundant reserve [1–6]. Therefore, Si is the one of the most attractive materials as an anode for lithium ion battery. Two main problems should be solved for Si to be used as an anode commercially, which are low electrical conductivity and significant volume expansion (~300%) during Li insertion/extraction [7–12]. In order to enhance electronic conductivity, many researchers have been studied on several of Si-based electrodes. Carbon materials, including artificial graphite, natural

graphite, and hard carbon are widely applied for Si coating and the mixture of high carbon Si/carbon composite was synthesized [13–15]. However, it was shown a limitation in the number of times the cycle test. It is because of the lack of enough change in volume of the internal volume of Si. Core–shell structural Si/C composites prepared by the coating of polymer delivered outstanding electrochemical performance, such as good rate capability and a long cycling life, as anode for LIBs [6,13–15]. Yi's group has synthesized a C-Si and C-Si@G and shown the performance as an anode for LIB. It was clearly seen that the Si/C could only deliver ~617 mAh/g at 0.5 A/g after 100 cycles. The charge specific capacity of C-Si@G at ~1987 mAh/g under the same rates. Other researchers have reported that the specific capacity for porous Si/C anode is 600~750 mAh/g for LIB after 100 cycles [2,4,13,14]. It is confirmed that carbon materials in the silicon–carbon composite can improve the electronic conductivity of composite. However, it is not enough for carbon to play as a role of buffer the huge volume expansion caused by the processes of intercalating lithium ions in silicon.

New types of carbon have been explored to improve the cycle ability and the electrochemical performance due to their high surface area and good electrical conductivity. Many researchers have studied carbon nanomaterials, such as carbon nanofiber (CNF), a novel one-dimensional (1D) carbon nanomaterial, graphene, and carbon nanotubes (CNTs) [16,17]. Especially, several types of CNF have been manufactured from different sources, which also demonstrated good electrochemical performance [18,19]. However, most of the CNFs are from non-renewable precursors consequently limiting their large-scale application. Therefore, finding low-cost and renewable resources to manufacturing high performance CNF materials is a pressing problem for every researcher. Also, reducing the consumption of fossil fuel resources should be considered. Recently, biomass has become more attractive in preparation of useful carbonaceous materials as a bountiful renewable resource in nature. Biomass sources such as catkin, lignin, alginate, and wood sawdust have demonstrated excellent electrochemical performance as electrode materials for energy applications [20–25]. Some biomass materials such as pollen, lignin, chitin, cellulose, and catkin have been studied on batteries and supercapacitors [26–30]. They have many advantages of inexpensive, abundant natural resources, renewable, and huge specific surface area. Besides, they could directly serve as both a template with porous structure for LIB and a precursor for the preparation of carbon microfibers by simple carbonization [31,32]. Biomass is not widely applied as an anode for LIB. These day, Chen's group has reported that HPC@Si@GS shows high rate capability that the electrode delivers a high and stable capacity of 435 mAh/g at a high current density of 1.6 A/g. When the electrode is measured at original current density of 0.1 A/g, it can deliver a capacity of 1003 mAh/g after the subsequent 100 cycles [1]. Zhu's group has investigated that the Si@C@CNT electrode exhibits a specific capacity of 620 mAh/g at extremely high charging rate of 7.50 A/g. Furthermore, the Si@C@CNT-G electrode exhibits the capacity of 420 mAh/g at the rate of 0.2 C after 100 cycles [2]. MW is the one of the biomass sources and biomass has been studied as a supercapacitor. Recently, there are research papers that biomass has good conductivity, and there are also research publications applied to sulfur batteries. However, biomass is not yet widely used in LIB.

In this study, we used MW as a template with carbon porous structure and a precursor to prepare HCMT by simple carbonization. HCMT can provide large surface area to load Si particles and buffer space to cushion the enough volume expansion for Si. Therefore, Si was accommodated to MW and calcinated with low-cost carbon sources such as Chitosan (CTS), Agarose, and polyvinylidene fluoride (PVDF) in N_2 flow. Three different Si composites, HCMT@Si@C1, HCMT@Si@C1@C2 and HCMT@Si@C1@C3, were synthesized and discussed about electrochemical properties. Characterization for samples used after 100 cycle is in progress. In the future research, it will be the subject of future publication.

2. Materials and Methods

The silicon nanoparticles (Si NPs; APS = 50 nm, Alfa Aesar) were prepared and the milkweed (MW) was collected from nature, Korea. Natural MW was prepared by immersing in 10 mL of 2% polyvinylpyrrolidone (PVP; M.W. = 360,000, Sigma-Aldrich) for 30 min. Hollow carbon microtubes

(HCMT) were synthesized by simple carbonization of MW. Chitosan (CTS; medium molecular weight, Sigma-Aldrich) was added and stirred in 25 mL of 2% acetic acid for 2 h at 60 °C. 1 g of Si was dispersed in MW and stirred for 1 h. CTS solution was added into Si distributed to the inner and outer surface of MW, which was repeatedly dispersed by sonicating for 5 h at room temperature. Then, obtained mixtures of MW, Si, and CTS were dried to produce the powder for 24 h at 70 °C. HCMT@Si@C1 composite was prepared by simple carbonization of the powder at 400 °C for 2 h in nitrogen flow. After HCMT@Si@C1 composite was added into 6 wt.% PVDF ($(CH_2CF_2)n$, M.W. = 534,000, Sigma-Aldrich) in NMP solution (C_5H_9NO, 99%, Sigma-Aldrich) stirred for 12 h, it was dried and carbonized at 900 °C for 2 h in nitrogen flow to produce the HCMT@Si@C1@C3 composite. HCMT@Si@C1 composite was added into Agarose (Agarose; bioreagent, low EEO, Sigma-Aldrich) solution dissolved in deionized water (DI) and stirred for 2 h at 70 °C. A few drops of glutaraldehyde (glutaraldehyde; grade I, 25% in H2O, Sigma-Aldrich) was dropped and aged by sonication for 4 h at room temperature. HCMT@Si@C1@C2 composite was synthesized by carbonization 2 h at 900 °C in nitrogen flow after the solution was dried for overnight. The synthetic process of all materials is schematically illustrated in Figure 1.

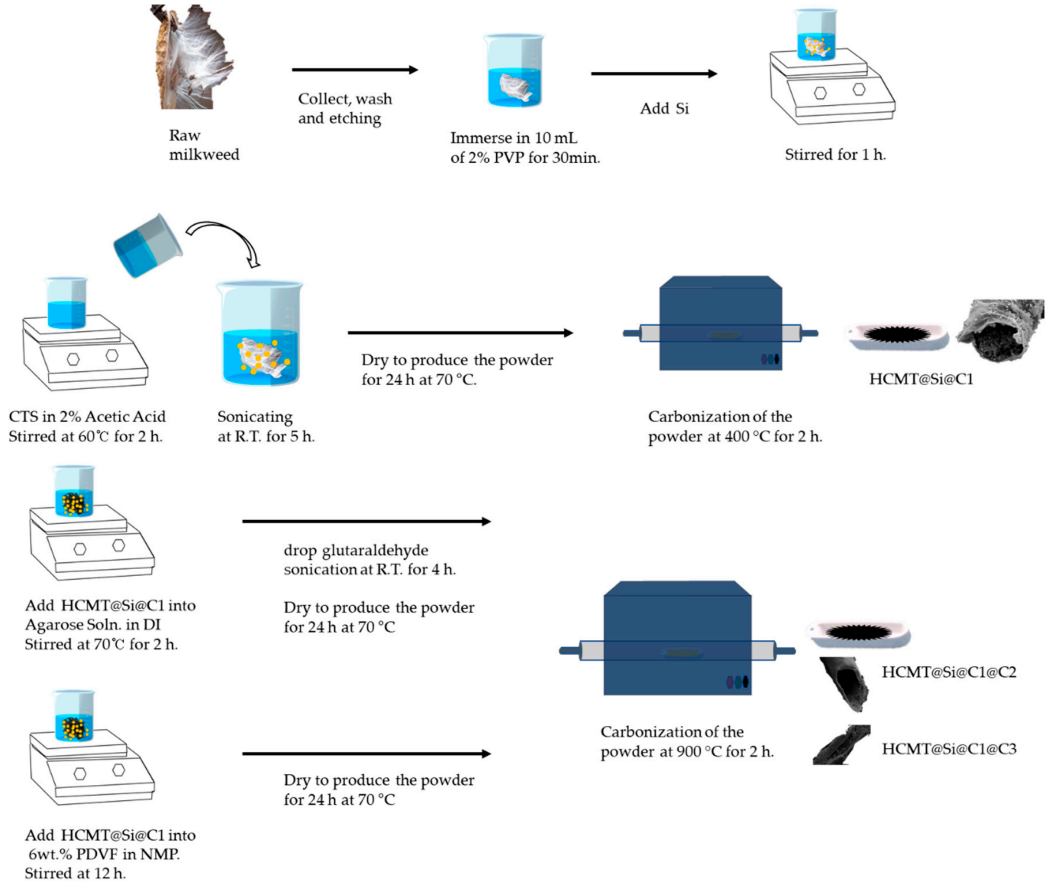

Figure 1. Schematics for preparation of the synthesized materials.

The synthesized materials were characterized by using a conventional X-ray diffractometer (XRD, X-pert PRO MPD, PANalytical, Netherlands) to analyze phase compositions and crystal structure. XRD was operated at θ–2θ scan mode (2θ range: 10–80° and scan speed: 1°/min) with Cu-$K_{\alpha 1}$ radiation (λ = 0.15408 nm) in continuous mode. The surface morphologies were measured by using scanning electron microscopy (SEM, Hitachi SU-70, Japan) operating at 15 kV. Samples were coated with platinum in order to increase their conductivity. The contents of carbon and Si for the carbon coated HCMT@Si composites were analyzed and calculated from thermogravimetric analysis (TGA, TA Q600, WATER,

USA) by heating from 25 °C to 700 °C with 10 °C/min at air atmosphere. The morphology and internal microstructure of carbon coated HCMT@Si composites were further observed by transmission electron microscopy (TEM, JEM 2100F, Jeol, Japan). TEM was operated at 200 kV acceleration voltage. Samples for TEM were prepared by dispersing the material in ethanol and drops of this dispersion were deposited onto carbon grids. The surface area of MW and HCMT was calculated by using N_2 adsorption/desorption isotherms. The particle size of MW and HCMT was characterized by particle and pore size analysis system (UPA-150, ASAP2010, AutoporeIV, Micromeritics, USA). The condition for degassing was at 400 °C for 12 h. In addition, the pore size of MW and HCMT was calculated by the BJH (Barrett-Joyner-Halenda) method.

For the working electrode, components were mixed with active material, conductive agent (carbon black, super P), and binder (PVDF) as weight ratio of 80:10:10. The mixed slurry was spread on the Cu foil using doctor blade with the thickness of 60 μm and dried at 70 °C for 2 h. All electrodes were served as the working electrode with 4 mg/cm^2 and a Li metal was served as counter electrode. The Celgard-2400 polypropylene-membrane was used as the separator. The electrolyte was 1.2 M $LiPF_6$ in an ethylene carbonate ethylene methyl carbonate with a volume ratio of 7:3 containing 10 vol.% FEC (fluoroethylene carbonate, Panax Etec Co., Ltd., ROK). CR2016 coin type half-cell was assembled for electrochemical properties of prepared electrodes in the glove box. The discharge/charge profiles of all the electrodes were measured by Galvanostat (WonAtech Co. Ltd., Korea) performing in the voltage range of 0.05 V to 1.5 V (vs Li^+/Li). The rate capabilities of all the electrodes were carried out at different current densities of 0.1, 0.5, 1, 2, 4, 1, and 0.5 A/g.

3. Results and Discussion

The XRD patterns of commercial Si (~50 nm), HCMT, HCMT@Si@C1, HCMT@Si@C1@C2, and HCMT@Si@C1@C3 are shown in Figure 2. HCMT displays a broad feature at 22.8° and 44.5°, indicating that carbon structure is dominant in the obtained HCMT. It was reported that the peak for willow catkins, wheat straw and cotton fibers around 21.7° should arise from the cellulose they owned and shift to the right a little by increasing the temperature of carbonization [23,33]. In comparison with Si, carbon coated HCMT@Si composites show sharp peaks of Si with reduced peak intensity. The five peaks at 28.6°, 47.4°, 56.3°, 69.3°, and 77.3° for Si and all prepared materials correspond to the characteristic peaks of (111), (220), (311), (400), and (331) crystal planes of Si. Besides, additional broad peak at 21.2° which is typical amorphous carbon and there are no impurity peaks for synthesized materials. This is the evidence that Si is well dispersed in HCMT and HCMT@Si is coated by carbon without the change of phase compositions for Si and carbon coated HCMT@Si by synthesis.

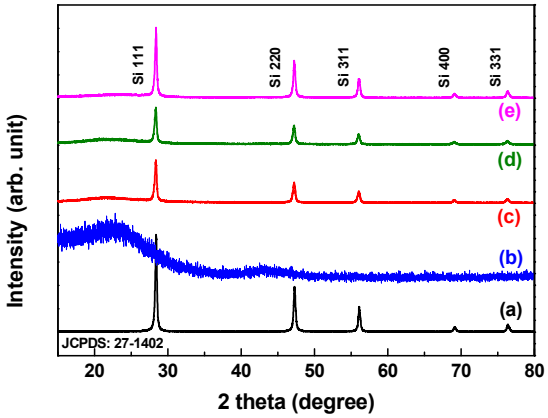

Figure 2. XRD patterns of the (**a**) Si; (**b**) HCMT; (**c**) HCMT@Si@C1; (**d**) HCMT@Si@C1@C2; (**e**) HCMT@Si@C1@C3.

Figure 3a depicts the surface area of raw MW and HCMT using N_2 adsorption/desorption isotherm. BET surface area for raw MW and HCMT was obtained with 12.97 and 143.64 m^2/g, respectively.

The Significant hysteresis was shown for HCMT in Figure 3a. It is common that the adsorbed nitrogen gas is not discharged as much as it is adsorbed during desorption. Significant hysteresis can be explained that gas is combined with the sample surface and remained. It is because the pore shape is like the bottle neck as well. An average pore size was calculated by BJH method from Figure 3b. The obtained average pore size was 7.61 and 6.19 nm for raw MW and HCMT. After calcination MW, BET surface area increased 10 times while an average pore size decreased slightly.

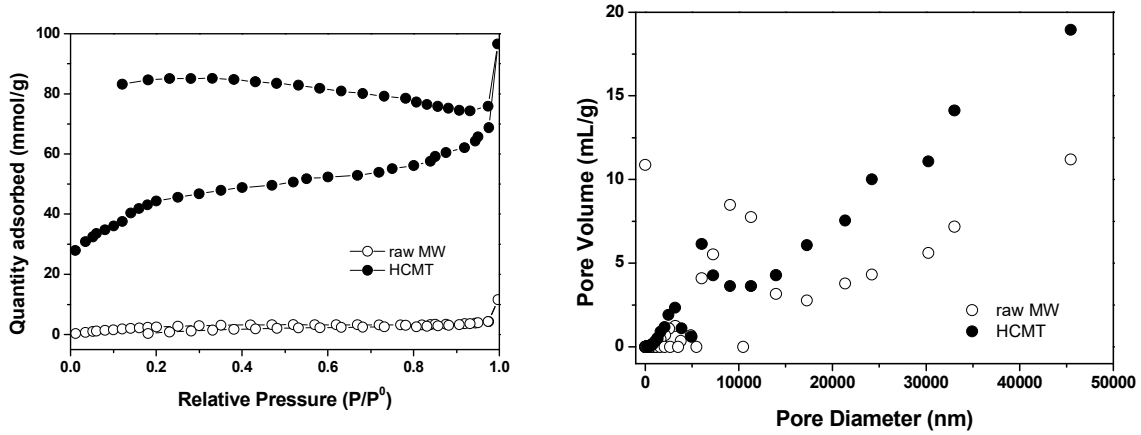

Figure 3. Particle and pore size analysis: (**a**) BET surface area; (**b**) pore size of raw MW and HCMT calculated by the BJH method.

Figure 4 shows SEM images of all synthesized materials including MW and HCMT. A MW has a hollow structure and a smooth surface with a diameter of 17–20 μm in Figure 4a. MW was carbonized with calcination in nitrogen atmosphere at 400 to 900 °C with 5 °C/min for 2 h. The hollow structure has an average diameter of about 10 μm and a wall thickness of about 650 nm as observed in Figure 4b. The diameter observed by SEM is different from the pore size by BJH. The pore size calculated by BJH means the average value of pores on the surface of hollow carbon tube, while the value from SEM is the diameter of hollow carbon tube. Usually the calculated range by BJH is up to 300 nm. The diameter of the micro-sized tube is not counted in the BJH calculation. As shown in Figure 4c–e. The hollow microtube structure of MW was sustained after carbon sources such as CTS, agarose, and PVDF on the outside of surface MW@Si were carbonized. Si particles were entered into the wall of MW and were fastened. It is indicated that Si particles were dispersed in the hollow tube and fixed in MW played as a role of an anode template which has a buffer void. In order to investigate Si particle were successfully wrapped by carbon and dispersed into HCMT, TEM, and TEM-element mapping of HCMT@Si@C1@C3 were carried out.

In Figure 5a, it is shown that carbon was deposited on the surface of Si particles in a form of a nanometer thick layer of carbon. The thickness of carbon layer is measured to be about 10 nm. TEM-element mapping images of HCMT@Si@C1@C3 showed the presence of Si, C and O elements in Figure 5b.

As shown in Figure 6, TGA curves for Si, HCMT@Si@C1, HCMT@Si@C1@C2, and HCMT@Si@C1@C3 were measured at a heating rate of 10 °C/min in air atmosphere. Weight loss in the curves is due to the combustion of carbon in the composite. On the other hand, slow increase of Si is ascribed to the oxidation of Si [1]. Major mass reduction was begun above 500 °C and the weight loss was mainly occurred between 550 °C and 650 °C. It can be explained that the oxidation of carbon in a sample reacted with oxygen atom. These results confirm that the weight loss of carbonized material increased with temperature and carbonized material was degraded around 650 °C completely. The remaining weight shows Si content in each sample and 77.8 wt.%, 77.2 wt.%, and 59.4 wt.% of HCMT@Si@C1, HCMT@Si@C1@C2, and HCMT@Si@C1@C3.

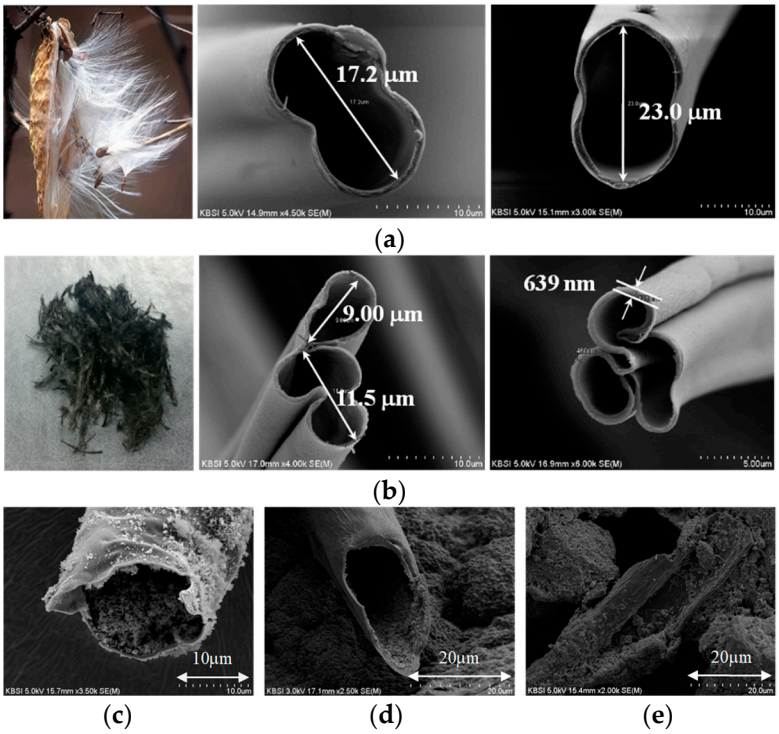

Figure 4. SEM images: (**a**) MW; (**b**) HCMT; (**c**) HCMT@Si@C1; (**d**) HCMT@Si@C1@C2; (**e**) HCMT@Si@C1@C3.

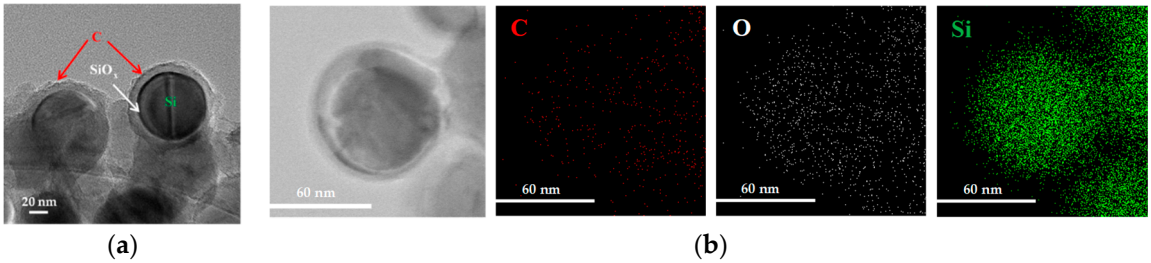

Figure 5. (**a**) TEM images; (**b**) TEM-element mapping images of HCMT@Si@C1@C3.

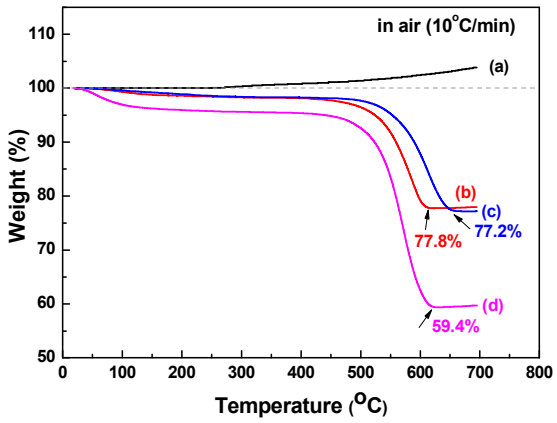

Figure 6. TGA curves recorded for (**a**) Si; (**b**) HCMT@Si@C1; (**c**) HCMT@Si@C1@C2; (**d**) HCMT@Si@C1@C3.

The cyclic performance of all synthesized materials for the subsequent 100 discharge/charge cycles was measured at 0.1 A/g (1st~5th cycle) and 0.5 A/g (6th~100th cycle) as shown in Figure 7a. Many researchers reported that Si electrode has very low charge capacity with retention of below 5% after 100 cycles [1]. When capacity rate increases from 0.1 to 0.5 A/g the capacity for carbon coated HCMT@Si

composites was decreased dramatically and was increased after 5 to 7th cycle at 0.5 A/g. The similar phenomenon of capacity increasing has been reported [1,34–37], which may be ascribed to the activation gradually of silicon without completely reaction in the composite electrode during the subsequent discharge/charge cycles. Other researchers explained that the dramatic increasing in charge capacity maybe attributed to a layer of gelatinous material that forms on the surface of the electrodes. That can provide additional capacity. Otherwise, the original SEI film cracks to generate a new thinner SEI film which leads to an increased capacity [8,38]. As shown in Figure 7a, HCMT@Si@C1, HCMT@Si@C1@C2, and HCMT@Si@C1@C3 electrodes have initial capacity of 764, 1038, and 1391 mAh/g at 0.5 A/g. Furthermore, the retention value for materials has 82%, 75% and 67% of the initial capacity after 100 charge/discharge cycles. The capacity of HCMT@Si@C1 has high retention of 82% which reveals good stability and a good candidate as an anode template of HCMT having inner void, while it was obtained low capacity of 632 mAh/g relatively after 100 cycles. The result of cycle performance for composites implies their stable energy storage processes during long cycle test. It can be inferred that HCMT can remarkably improve cycle stability as playing a role of void buffer.

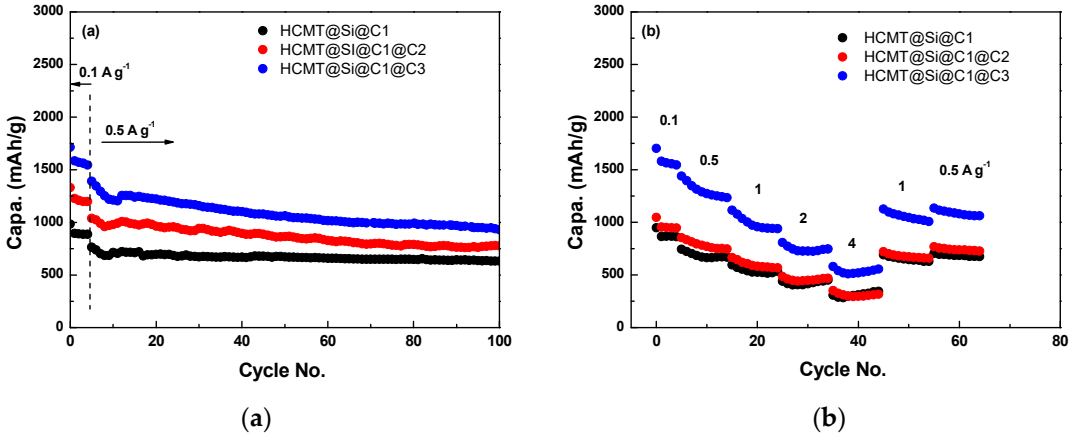

(**a**) (**b**)

Figure 7. (**a**) Cyclic curves HCMT@Si@C1, HCMT@Si@C1@C2, and HCMT@Si@C1@C3 electrodes for 100 cycles; (**b**) Rate capability of HCMT@Si@C1, HCMT@Si@C1@C2, and HCMT@Si@C1@C3 electrodes.

In comparison with HCMT@Si@C1 electrode, HCMT@Si@C1@C2 and HCMT@Si@C1@C3 electrodes were shown remarkably enhanced capacity of 776 and 932 mAh/g after 100 cycles, respectively. It means the electronic conduction of HCMT@Si composites was improved by using the combination of C1 and C3 among variety of carbon sources. The HCMT in composites provides a large interfacial area and stabilizing the morphology and structure of the Si anode. Figure 7b shows the rate capability of HCMT@Si@C1, HCMT@Si@C1@C2, and HCMT@Si@C1@C3 electrodes cycled at different rates of 0.1, 0.5, 1, 2, 4, 1, and 0.5 A/g. The capacity of HCMT@Si@C1, HCMT@Si@C1@C2 and HCMT@Si@C1@C3 electrodes was decreased with higher current density. All composites exhibited stable capacity at high current density and HCMT@Si@C1@C3 obtained high capacity of 744 mAh/g at 2 A/g and 555 mAh/g at 4 A/g. The capacity of 1232 mAh/g was recovered to 1061 mAh/g with retention of 86% when the current density decreases back to 0.5 A/g. The rate capability and stability of HCMT@Si@C1 was very excellent compared with HCMT@Si@C1@C2 and HCMT@Si@C1@C3 as shown in Figure 7. However, the capacity of HCMT@Si@C1 was necessary to be improved and the capacity of HCMT@Si@C1@C3 was obtained much higher than that of HCMT@Si@C1 and HCMT@Si@C1@C2. For the HCMT@Si@C1@C3, the excellent cyclic performance and rate capability obtained are mainly attributed to the hard template of hollow microtube structure and the outer material. Si particles are adjoined on the surface of hollow microtube structure and fixed on the inner wall of HCMT mostly. Then obtained HCMT@Si particles are coated by carbonization from variety of carbon sources to improve conductivity and stable structure. The hollow microtube structure provides void when Si expands repeating discharge/charge cycle, which protects from cracking and damage of cell. Also, among carbonized material from several

carbon sources, carbonization of C1 and C3 might be coated the Si surface evenly and harder than C1, the combination of C1 and C2. Also, the combination of C1 and C3 improved electronic conductivity to the transport of lithium ion.

4. Conclusions

Carbon coated HCMT@Si composites were synthesized by simple carbonization of MW having hollow microtube structure from nature. The content of Si for each sample shows 60~78% from TGA result. SEM results show that Si is adjoined on the surface and inside of MW. Synthesized carbon coated HCMT@Si composites display much better electrochemical performance than Si which has a theoretical high specific capacity but poor cycle performance as known popularly. Although volume expansion and shrinkage of Si are repeated during the insertion and extraction of lithium ions, it shows improving capacity retention because the void in hollow microtube structure of milkweed serve as a buffer for volume expansion. Charge/Discharge was performed 100 cycles (5 cycles with 100 mAh/g, 95 cycles with 0.5 mAh/g) and the capacity for HCMT@Si@C1@C3 was obtained ~950 mAh/g after 100 cycles with 0.5 mAh/g. HCMT@Si@C1@C3 showed excellent cycling performance and high degree of reversibility because of better electronic conductivity than others. It demonstrated again the great potential for energy storage applications.

Author Contributions: Conceptualization, Project administration, Preparation, experiment, Writing—original draft, and Writing—review and edition, E.H.C.; Conceptualization, Project administration, review and editing, E.D.J.; Data results analysis, J.P.K., H.G.K., and S.-J.L.; funding acquisition, J.-S.B.; Material and resource support, J.-M.C. All authors have read and agreed to the published version of the manuscript.

Funding: This research was funded by the National Research Foundation of Korea (NRF), grant number ICT (NRF-2018M1A2063349).

Conflicts of Interest: The authors declare no conflict of interest.

References

1. Chen, H.; He, S.; Hou, X.; Wang, S.; Chen, F.; Qin, H.; Xia, Y.; Zhou, G. Nano-Si/C microsphere with hollow double spherical interlayer and submicron porous structure to enhance performance for lithium-ion battery anode. *Electrochim. Acta* **2019**, *312*, 242–250. [CrossRef]
2. Zhu, X.; Choi, S.; Tao, R.; Jia, X.; Lu, Y. Building high-rate silicon anodes based on hierarchical Si@C@CNT nanocomposite. *J. Alloys Comp.* **2019**, *791*, 1105–1113. [CrossRef]
3. Han, X.; Zhang, Z.; Chen, H.; You, R.; Zheng, G.; Zhang, Q.; Wang, J.; Li, C.; Chen, S.; Yang, Y. Double-shelled microscale porous Si anodes for stable lithium-ion batteries. *J. Power Sources* **2019**, *436*, 226794. [CrossRef]
4. Park, J.B.; Lee, K.H.; Jeon, Y.J.; Lim, S.H.; Lee, S.M. Si/C composite lithium-ion battery anodes synthesized using silicon nanoparticles from porous silicon. *Electrochim. Acta* **2014**, *133*, 73–81. [CrossRef]
5. Mu, G.; Ding, Z.; Mu, D.; Wu, B.; Bi, J.; Zhang, L.; Yang, H.; Wu, H.; Wu, F. Hierarchical void structured Si/PANi/C hybrid anode material for high-performance lithium-ion batteries. *Electrochim. Acta* **2019**, *300*, 341–348. [CrossRef]
6. Yi, X.; Yu, W.J.; Tsiamtsouri, M.A.; Zhang, F.; He, W.; Dai, Q.; Hu, S.; Tong, H.; Zheng, J.; Zhang, B.; et al. Highly conductive C-Si@G nanocomposite as a high-performance anode material for Li-ion batteries. *Electrochim. Acta* **2019**, *295*, 719–725. [CrossRef]
7. Hua, Z.G.; Tana, Z.Y.; Lina, Z.; Chena, J.; Suna, F.; Tanga, X.; Zhenga, R.T.; Chen, Y.C.; Cheng, G.A. Dynamic processes in Si and Si/C anodes in lithium-ion batteries during cycling. *J. Electroanal. Chem.* **2019**, *839*, 187–194. [CrossRef]
8. Lee, S.Y.; Choi, Y.; Kwon, S.H.; Bae, J.S.; Jeong, E. Cracking resistance and electrochemical performance of silicon anode on binders with different mechanical characteristics. *J. Ind. Eng. Chem.* **2019**, *74*, 216–222. [CrossRef]
9. Lee, S.Y.; Choi, Y.; Hong, K.S.; Lee, J.; Kim, J.Y.; Bae, J.S.; Jeong, E. Influence of EDTA in poly(acrylic acid) binder for enhancing electrochemical performance and thermal stability of silicon anode. *Appl. Surf. Sci.* **2018**, *447*, 442–451. [CrossRef]

10. Jain, A.; Jayaraman, S.; Ulaganathan, M.; Balasubramanian, R.; Aravindan, V.; Srinivasan, M.P.; Madhavi, S. Highly mesoporous carbon from Teak wood sawdust as prospective electrode for the construction of high energy Li-ion capacitors. *Electrochim. Acta* **2017**, *228*, 131–138. [CrossRef]
11. Han, X.; Chen, H.; Liu, J.; Liu, H.; Wang, P.; Huang, K.; Li, C.; Chen, S.; Yang, Y. A peanut shell inspired scalable synthesis of three-dimensional carbon coated porous silicon particles as an anode for lithium-ion batteries. *Electrochim. Acta* **2015**, *156*, 11–19. [CrossRef]
12. Nguyen, H.T.; Yao, F.; Zamfir, M.R.; Biswas, C.; So, K.P.; Lee, Y.H.; Kim, S.M.; Cha, S.N.; Kim, J.M.; Pribat, D. Highly interconnected Si nanowires for improved stability Li-ion battery anodes. *Adv. Energy Mater.* **2011**, *1*, 1154–1161. [CrossRef]
13. Tian, H.; Tan, X.; Xin, F.; Wang, C.; Han, W. Micro-sized nano-porous Si/C anodes for lithium ion batteries. *Nano Energy* **2015**, *11*, 490–499. [CrossRef]
14. Zuoa, X.; Wang, X.; Xia, Y.; Yin, S.; Ji, Q.; Yang, Z.; Wang, M.; Zheng, X.; Qiu, B.; Liu, Z.; et al. Silicon/carbon lithium-ion battery anode with 3D hierarchical macro-/mesoporous silicon network: Self-templating synthesis via magnesiothermic reduction of silica/carbon composite. *J. Power Sources* **2019**, *412*, 93–104. [CrossRef]
15. Prakash, S.; Zhang, C.; Park, J.D.; Razmjooei, F.; Yu, J.S. Silicon core-mesoporous shell carbon spheres as high stability lithium ion battery anode. *J. Colloid Interface Sci.* **2019**, *534*, 47–54. [CrossRef]
16. Li, W.; Zeng, L.; Wu, Y.; Yu, Y. Nanostructured electrode materials for lithium-ion and sodium-ion batteries via electrospinning. *Sci. China Mater.* **2016**, *59*, 287–321. [CrossRef]
17. Kaskhedikar, N.A.; Maier, J. Lithium storage in carbon nanostructures. *Adv. Mater.* **2009**, *21*, 2664–2680. [CrossRef]
18. Chen, C.; Lu, Y.; Ge, Y.Q.; Zhu, J.D.; Jiang, H.; Li, Y.Q.; Hu, Y.; Zhang, X. Synthesis of nitrogen-doped electrospun carbon nanofibers as anode material for high-performance sodium-ion batteries. *Energy Technol.* **2016**, *4*, 1440–1449. [CrossRef]
19. Wang, Q.F.; Yu, Y.; Ma, J.; Zhang, N.; Zhang, J.J.; Liu, Z.H.; Cui, G. Electrospun melamine resin-based multifunctional nonwoven membrane for lithium ion batteries at the elevated temperatures. *J. Power Sources* **2016**, *327*, 196–203. [CrossRef]
20. Zhang, Y.; Zhao, Y.; Konarov, A.; Li, Z.; Chen, P. Effect of mesoporous carbon microtube prepared by carbonizing the poplar catkin on sulfur cathode performance in Li/S batteries. *J. Alloy. Comp.* **2015**, *619*, 298–302. [CrossRef]
21. Liu, L.; Feng, R.; Pan, Y.; Zheng, X.; Bai, L. Nanoporous carbons derived from poplar catkins for high performance supercapacitors with a redox active electrolyte of pphenylenediamine. *J. Alloy. Comp.* **2018**, *748*, 473–480. [CrossRef]
22. Wang, K.; Zhao, N.; Lei, S.; Yan, R.; Tian, X.; Wan, J.; Song, Y.; Xu, D.; Guo, Q.; Liu, L. Promising biomass-based activated carbons derived from willow catkins for high performance supercapacitors. *Electrochim. Acta* **2015**, *166*, 1–11. [CrossRef]
23. Ma, Y.; Zhao, J.; Zhang, L.; Zhao, Y.; Fan, Q.; Li, X.; Hu, Z.; Huang, W. The production of carbon microtubes by the carbonization of catkins and their use in the oxygen reduction reaction. *Carbon* **2011**, *49*, 5292–5297. [CrossRef]
24. Zhang, Z.; Wang, Y.; Ren, W.; Tan, Q.; Chen, Y.; Li, H.; Zhong, Z.; Su, F. Scalable synthesis of interconnected porous silicon/carbon composites by the Rochow reaction as high-performance anodes of lithium ion batteries. *Angewandte Chem.* **2014**, *53*, 5165–5169. [CrossRef]
25. Wang, Y.Q.; Zhang, Z.Q.; Zhu, S.Y.; Sun, D.Y.; Jin, Y.C. Enteromorpha prolifera-derived carbon as a high-performance cathode material for lithium–sulfur batteries. *J. Appl. Electrochem.* **2017**, *47*, 631–639. [CrossRef]
26. Li, Y.; Wangn, G.; Wei, T.; Fann, Z.; Yan, P. Nitrogen and sulfur co-doped porous carbon nanosheets derived from willow catkin for supercapacitors. *Nano Energy* **2016**, *19*, 165–175. [CrossRef]
27. Liu, P.; Wang, Y.; Liu, J. Biomass-derived porous carbon materials for advanced lithium sulfur batteries. *J. Energy Chem.* **2019**, *34*, 171–185. [CrossRef]
28. Wanga, K.; Songa, Y.; Yana, R.; Zhaoa, N.; Tiana, X.; Lia, X.; Guoa, Q.; Liu, Z. High capacitive performance of hollow activated carbon fibers derived from willow catkins. *Appl. Surf. Sci.* **2017**, *394*, 569–577. [CrossRef]
29. Wang, K.; Yan, R.; Zhao, N.; Tian, X.; Li, X.; Lei, S.; Song, Y.; Guo, Q.; Liu, L. Bio-inspired hollow activated carbon microtubes derived from willow catkins for supercapacitors with high volumetric performance. *Mater. Lett.* **2016**, *174*, 249–252. [CrossRef]

30. Su, X.L.; Cheng, M.Y.; Fu, L.; Yang, J.H.; Zheng, X.C.; Guan, X.X. Superior supercapacitive performance of hollow activated carbon nanomesh with hierarchical structure derived from poplar catkins. *J. Power Sources* **2017**, *362*, 27–38. [CrossRef]
31. Tao, L.; Huang, Y.; Zheng, Y.; Yang, X.; Liu, C.; Di, M.; Larpkiattaworn, S.; Nimlos, M.R.; Zheng, Z. Porous carbon nanofiber derived from a waste biomass as anode material in lithium-ion batteries. *J. Taiwan Ins. Chem. Eng.* **2019**, *95*, 217–226. [CrossRef]
32. Fromm, O.; Heckmann, A.; Rodehorst, U.C.; Frerichs, J.; Becker, D.; Winter, M.; Placke, T. Carbons from biomass precursors as anode materials for lithium ion batteries: New insights into carbonization and graphitization behavior and into their correlation to electrochemical performance. *Carbon* **2018**, *128*, 147–163. [CrossRef]
33. Teixeira, E.M.; Corre^a, A.C.; Manzoli, A.; Leite, F.L.; Oliveira, C.R. Cellulose nanofibers from white and naturally colored cotton fibers. *Cellulose* **2010**, *17*, 595–606. [CrossRef]
34. Mishra, K.; George, K.; Zhou, X.D. Submicron silicon anode stabilized by single-step carbon and germanium coatings for high capacity lithium-ion batteries. *Carbon* **2018**, *138*, 419–426. [CrossRef]
35. Lin, D.; Lu, Z.; Hsu, P.C.; Lee, H.R.; Liu, N.; Zhao, J.; Wang, H.; Liu, C.; Cui, Y. A high tap density secondary silicon particle anode fabricated by scalable mechanical pressing for lithium-ion batteries. *Energy Environ. Sci.* **2015**, *8*, 2371–2376. [CrossRef]
36. Chen, Y.; Hu, Y.; Shen, Z.; Chen, R.; He, X.; Zhang, X.; Zhang, Y.; Wu, K. Sandwich structure of graphene-protected silicon/carbon nanofibers for lithium-ion battery anodes. *Electrochim. Acta* **2016**, *210*, 53–60. [CrossRef]
37. Deng, L.; Cui, Y.; Chen, J.; Wu, J.; Baker, A.P.; Li, Z.; Zhang, X. A Core-shell Si@$NiSi_2$/Ni/C nanocomposite as an anode material for lithium-ion batteries. *Electrochim. Acta* **2016**, *192*, 303–309. [CrossRef]
38. Xu, Z.L.; Zhang, B.; Kim, J.K. Electrospun carbon nanofiber anodes containing monodispersed Si nanoparticles and graphene oxide with exceptional high rate capacities. *Nano Energy* **2014**, *6*, 27–35. [CrossRef]